A photosensitive Cr^{3+} center in photorefractive $Bi_{12}SiO_{20}$ crystals co-doped with chromium and phosphorus

Ijaz Ahmad [1], Vera Marinova [1,2] Henk Vrielinck [3], Freddy Callens [3] and Etienne Goovaerts [1,a]

[1] *Experimental Condensed Matter Physics, Physics Department, University of Antwerp, Universiteitsplein 1,B-2610 Antwerpen, Belgium*

[2] *Institute of Optical Materials and Technologies, Bulgarian Academy of Sciences, 1784 Sofia, Bulgaria*

[3] *Department of Solid State Sciences, Ghent University, Krijgslaan 281–S1, B-9000-Gent, Belgium*

ABSTRACT:

A trigonal Cr^{3+} ($3d^3$) defect in sillenite type $Bi_{12}SiO_{20}$ crystals co-doped with chromium and phosphorus has been identified by means of multi-frequency X-band (9.4 GHz), Q-band (35 GHz) and W-band (94 GHz) electron paramagnetic resonance (EPR). A consistent analysis of the observed spectra and their angular dependence was reached using an S=3/2 spin Hamiltonian with axial symmetry around a <111> crystallographic direction, an isotropic g-value $g = 1.983$, and a zero field splitting parameter $B_2^0 = 0.1950$ cm^{-1}. The spectra are attributed to a chromium ion in the unusual Cr^{3+} valence replacing a substitutional Si^{4+} in tetrahedral oxygen coordination. Evidence is found that the symmetry lowering from tetrahedral to trigonal is not spontaneous but induced by an associated defect, for which a P^{5+} ion in a nearest-neighbor Si^{4+} site is the most plausible candidate. Optical excitation results in a reversible charge transfer process directly correlated with a photochromic effect: near-UV light leads to a strong reduction of the Cr^{3+} EPR signals, and induces a broad band at 675 nm in the absorption spectrum, and both effects are reversed under red light excitation.

[a] Corresponding author, electronic address: Etienne.Goovaerts@ua.ac.be

1. INTRODUCTION

Bismuth oxide compounds such as the sillenite-type $Bi_{12}MO_{20}$ (BMO, where M= Si, Ge, Ti) crystals are being extensively studied because of their potential applications including dynamic holography, optical information processing, optical phase conjugation and real-time interferometry.[1-5] These materials are technologically important because of their photorefractive (PR) properties caused by light induced charge carrier migration and consecutive trapping by suitable defects.[6] Point defects, either intrinsic or extrinsic, play a fundamental role in the PR behavior. Introducing suitable dopants is an effective way to alter the PR response of BMO crystals taking into account the requirements of specific applications. The defect identification, including the dopant ions involved, their valence and local symmetry, as well as possibly associated intrinsic defects that participate in the PR effect, is essential because this information may guide the efforts for optimization of the synthesis conditions to obtain the intended material properties.

Among the intrinsic defects, the antisite defect, consisting of a bismuth ion on a tetrahedral M^{4+} site, proved to be very important for the PR effect in undoped crystals. Under illumination in the visible or near UV region an electron of the antisite Bi^{3+} center, Bi_M^{3+}, is excited to the conduction band and the remaining hole is localized mainly on the four oxygen ligands forming a hole-trapped antisite center, the Bi_M^{4+} defect. This was extensively studied by optical absorption spectroscopy [7-8] identifying bands corresponding to the Bi_M^{3+} and Bi_M^{4+} defects. Phosphorus doping was observed to effectively bleach these bands, showing that it strongly reduces the concentration of Bi antisite centers.[7,9-11] Optically detected magnetic resonance (ODMR) was used to study the electronic state and the symmetry of the Bi_M^{4+} defect.[12,13] However, only recently direct detection of the electron paramagnetic resonance (EPR) spectra was reported.[14] In the three sillenite hosts an exploratory study of the effect of doping and illumination on the concentration of Bi_M^{4+} was performed, and $Bi_{12}SiO_{20}$ (BSO) co-doped with Cr and P was found to be an exception in this series, since the Bi_{Si}^{4+} defect was found to be absent in this crystal before as well as after illumination.

It has been previously reported that chromium in BSO and $Bi_{12}GeO_{20}$ (BGO) crystals occupies the tetrahedral metal M^{4+} sites in the oxidation states Cr^{5+} and Cr^{4+} and that both reduction under vacuum annealing and illumination pushes the balance towards

Cr^{4+} (Refs. 15-17). Egorysheva *et al*. have also reported the existence of both these oxidation states in $Bi_{12}TiO_{20}$ (BTO) single crystals doped with chromium.[18] Furthermore, it was proposed that besides the tetrahedrally coordinated Cr^{4+} and Cr^{5+}, chromium may be incorporated in BSO and BGO at an interstitial site with orthorhombic symmetry.[19] Chromium related defects have been also reported in eulitine-type $Bi_4Ge_3O_{12}$ single crystals,[20,21] in which the Cr^{3+} ion in the octahedrally coordinated Bi site was found as a minority species.[20] The presence of chromium in the trivalent state has not been unambiguously demonstrated in the sillenite-type BMO crystals. Indeed, an early report on Cr^{3+} in chromium-only doped BGO and BSO [22] was revoked in a subsequent study,[15] and insufficient evidence was available for other Cr^{3+} assignments.[23,24] In particular, the assignment in [23] of a weakly anisotropic X-band EPR spectrum in chromium-only doped BSO was proposed without specific analysis.

Grabmaier and Oberschmidt [7] demonstrated that phosphorus doping in BGO and BSO leads to tetrahedral site occupation in the P^{5+} charge state and this dopant acts as an electron donor. When P is introduced in the BMO sillenite matrix, the concentration of oxygen vacancies decreases substantially (caused by a reduced concentration of defective $[BiO_4]$ polyhedra), which decreases the intrinsic donor concentration while the photochromic effect is also quenched.[9-11] A broad absorption band centered at 1.8 eV formed after band-edge illumination was attributed to the metastable P^{4+} center formed by electron trapping at P^{5+} (Ref. 10). In the case of Cr and P co-doping, the phosphorus was found to influence the Cr^{5+}/Cr^{4+} oxidation state, increasing the fraction of Cr^{4+} (Ref. 25).

Most of the reported work on the chromium related defects in these crystalline hosts was devoted to optical absorption spectroscopy, which has a direct relationship with the induced photorefractivity.[8,16-18,22,25,26] This approach, however, offers only limited information on the microscopic structure of the impurity centers that contribute to the PR properties. A combination with paramagnetic resonance techniques is a powerful approach to obtain information on the nature of these centers, such as the valence of ions, their local symmetry and the possible involvement of intrinsic defects.[27]

In this paper, we present a detailed study of a photosensitive chromium-related center in $Bi_{12}SiO_{20}$ co-doped with chromium and phosphorus (BSO:Cr+P), using EPR

spectroscopy at X-Band (9.4 GHz), Q-band (35 GHz) and W-band (94 GHz) microwave frequencies. This approach yields the first unequivocal identification of a Cr^{3+} defect in the bismuth sillenites. Bleaching and recovery of the EPR signal of these centers under optical excitation is demonstrated and correlated with light-induced changes in the optical absorption spectra.

2. CRYSTAL STRUCTURE AND EXPERIMENTAL PROCEDURES

$Bi_{12}SiO_{20}$ crystals belong to the sillenite family of materials with the space symmetry I23 with a body centered cubic unit cell (a = 10.102 Å), which contains 24 Bi^{3+} ions, 2 Si^{4+} ions and 40 O^{2-} ions (nominal valences). Two structural elements can be distinguished (see Fig.1), the SiO_4 regular tetrahedron and the BiO_7 polyhedron.[28] The former exists at the corners and at the centre of the cubic unit cell. In the BiO_7 polyhedron, each of the Bi^{3+} ions is surrounded by 7 oxygen atoms and is coordinated in a pseudo-octahedral configuration, in which the oxygen atom at one corner is replaced by two atoms at somewhat larger distance (see Fig. 1(a)).

BSO single crystals were grown in air by the Czochralski method from a melt containing a mixture of high purity (99.9999%) oxides including Bi_2O_3 and SiO_2 in a 6:1 molar ratio.[29] Platinum crucibles of 60 mm in diameter and 80 mm in height were used as containers. The crystals were grown in a <001> direction under conditions of low temperature gradient over the solution (5-7 ºC/cm), at a growth rate of 0.7 mm/h and a rotation rate of 20 rpm. Fully facetted and optically homogeneous crystals of 35 mm in diameter and 50 mm in height were obtained. The starting chromium and phosphorus dopants were introduced into the melt solution in the form of the oxides Cr_2O_3 and P_2O_5, respectively. The analysis by atomic absorption spectrometry shows that they are present in the crystal at concentrations of [Cr] = 4.9×10^{18} cm^{-3} and [P] = $4.4\times10^{19}cm^{-3}$. This corresponds to relative concentrations [Cr]/[Si] = 0.25 % and [P]/[Si] = 2.2 %.

The orientation of the crystals was performed using X-ray diffraction (STOE four circle diffractometer) operating in transmission mode through a thinned extremity of boule pieces. Using a thin diamond plate, samples of suitable size that fit the X-band (~1.5 mm ×1.5 mm ×5 mm), Q-band (~1.2 mm ×1.2 mm ×2 mm) and W-band (~0.5 mm ×0.5 mm ×1.5 mm) sample tubes were cut with their long axis perpendicular to

a {110} plane. Before the measurements, the crystals were thermally annealed at 350 °C and slowly cooled to room temperature (RT). This could not be applied to the W-band samples (see below) because the glue used for mounting does not stand the treatment.
Continuous wave EPR measurements were carried out on oriented samples at X, Q and W-Band frequencies, on Bruker spectrometers (ESP300, and Elexsys E500 and E680, respectively), using 100 kHz field modulation. The instruments are equipped with dedicated Oxford liquid helium cryostats.

In the orientational study of the W-band EPR spectra the small crystal, (glued to a quartz tube) was fixed onto a rotating sample holder having digital readout for high angular precision (~0.1°). The sample was directly illuminated inside the cavity by means of an optical fiber. The quartz fiber was threaded through the sample holder and positioned about half a millimeter from the end face of the crystal. A Kr^{+}-ion laser (Spectra Physics) was used at selectable wavelengths in the range of 350 nm to 752 nm for sample illumination. The laser power at the fiber end was adjusted to ~ 30 mW.

Simulation and fitting of the EPR spectra were performed by means of the SIM (ESRFIT) program based on full diagonalization of the spin Hamiltonian matrix.[30]

Optical absorption spectra of thin polished plates cut from the studied BSO crystals were measured at T = 90 K in a liquid nitrogen cooled optical cryostat using a Varian Cary 5 spectrophotometer. For near UV and red light excitation of the sample inside the cryostat the Kr^{+}-ion laser mentioned above was used as a source.

3. EXPERIMENTAL RESULTS

A. EPR experiments

The X-band EPR spectrum of the as-grown sample measured at 10 K is shown in Fig. 1(a) when the magnetic field is oriented in a {110} plane along a direction close a <111> crystal axis. The intense narrow single line flanked by two shoulders (best visible in X-band) in the spectrum close to g = 2 has been previously reported in X-band EPR studies and attributed to Fe^{3+} residual impurities substituting at the Si^{4+} site.[31,32] The remaining resonance lines in the range from 100 mT to 320 mT show an anisotropic

behavior and are originating from a chromium related defect, as will be discussed below. One can see that the spectral resolution is limited due to the width of the resonance lines (~40 mT) and this hampers the precise determination of their field positions. Figs. 2(b) and 2(c), show the Q-band and W-band EPR spectra of the BSO:Cr+P sample for the same orientation of the magnetic field along a <111> crystal direction. The line widths are not drastically increased compared to the X-band measurements. However, at higher microwave frequencies a larger number of transitions is observed and both the splitting between the lines and the anisotropic shifts are in these cases much larger than the linewidth, providing a higher relative spectral resolution and allowing for a detailed analysis of the data.

Fig. 3 shows the full angular variation of the EPR transitions when the magnetic field is rotated in a {110} crystallographic plane in steps of 10°. The observed resonance line pattern is analyzed on the basis of an S = 3/2 spin Hamiltonian (SH) with trigonal symmetry along the local z-axis, z // <111> (in conventional notation [33]):

$$H = g\,\mu_B B.S + B_2^0\,O_2^0, \text{ with } O_2^0 = 3S_z^2 - S^2 \qquad (1)$$

The first term represents the Zeeman interaction, which is taken here to be isotropic. Indeed, the fitting of the angular variation data could not be significantly improved by the introduction of an axial g-anisotropy. The last term is the second-order zero field splitting (ZFS) contribution (with interaction parameter B_2^0 corresponding in the alternative ZFS notation to $D = 3\,B_2^0$). For an $S = 3/2$ system in trigonal symmetry only this second-order term appears, leading to axial symmetry for SH (1). Therefore the resonance field positions for each defect depend only on the angle between the trigonal axis and the applied magnetic field. The defect's trigonal axis may, however, be oriented along each of the four (pairs of) equivalent <111> directions in the cubic BSO crystal. For arbitrary magnetic field orientations, this results in four magnetically inequivalent sites, but when the magnetic field is rotated in a {110} plane, only three are observed. For two of them the defect axis is lying in the rotation plane at ±54.74° from a <100> direction, while the two out-of-plane orientations remain equivalent because they are related by mirror symmetry through this plane. As shown in Fig. 3, the experimental angular variation can be accurately described on the basis of SH (1) for the fitted

parameter values $g = 1.983 \pm 0.001$ and $B_2^0 = 0.1950 \pm 0.0004$ cm^{-1}. In Fig. 3, the diamonds correspond to the experimentally measured resonance field positions (solid and open diamonds for allowed and forbidden transitions, respectively), in very good agreement with the calculated ones that are indicated by open circles with size proportional to the transition multiplicity weighed probabilities. Moreover, the angular variations measured in the X- and Q-band (not shown) also fit well with calculations based on this SH.

Considering the accurate description obtained with spin S = 3/2, an identification as Cr^{3+} ($3d^3$,^4F ground state) in a crystal field of appropriate symmetry appears obvious. In particular, the isotropic g-value smaller than the free electron value, can result from quenching of the large angular momentum in the ground state by the crystal field. While this settles the chromium valence, two scenarios have been shown to be compatible with the SH parameters of this center, namely, either an octahedral [34] or a tetrahedral [35] coordination with a trigonal perturbation acting on the d^3 ion. These alternatives and their implications for the impurity site will be considered later (Sec. 4).

An additional point of interest in these EPR spectra is the absence of the intense single line reported for chromium doped bismuth sillenite crystals at $g \cong 1.938$ (see also the BSO:Cr spectrum in the inset of Fig. 2(c)). This line has been attributed to the Cr_{Si}^{4+} defect, a Cr^{4+} ion in tetrahedral coordination,[15] substituting for a Si^{4+} ion. While the Cr^{4+} state is dominant in chromium-only doped BSO, this is drastically altered by co-doping with phosphorus (at a 10-fold concentration compared to Cr), that has a preferred P^{5+} valence and thus can act as an electron donor to the Cr-ions. Co-doping with phosphorus thus drastically changes the state of the incorporated chromium ions. As discussed below this is also supported by the qualitatively different optical absorption spectra.

P-doping has previously been found to act as an electron donor in BMO crystals, shifting the Fermi-level upwards and possibly filling defect states in the band gap.[7,10] Also, the EPR spectrum of the antisite Bi_M^{4+} hole type defect is absent in BSO:Cr+P even after near-UV excitation, while we did observe it in a series of undoped and doped BMO crystals,[14] in particular in singly-doped BSO:Cr. Again this could be related to the donor activity of the P co-dopant, keeping the antisite centre in the diamagnetic Bi_M^{3+} state, but

also the concentration of available bismuth antisite ions is strongly reduced by P doping in these crystals, as previously reported.[7,9,10,11]

B. Effect of laser illumination

In order to study the charge transfer processes in BSO:Cr+P, EPR measurements were also performed after illumination of the samples. Illumination at wavelengths longer than 450 nm, even at low temperature, did not yield any detectable change in EPR or optical (see below) spectra of the annealed crystals. Fig. 4 shows the W-band EPR spectrum that was measured after *in situ* laser light excitation at 413 nm during 20 min (curve b), to be compared with the spectrum of the annealed crystal state (curve a). A strong reduction in EPR intensities and thus of the concentration of the Cr^{3+} related defect was observed. Assuming that the decrease results from the excitation of an electron to the conduction band which gets trapped at another site, this would be expected to result in the production of Cr^{4+} centers. It is however obvious from the absence of the typical line at $g \cong 1.938$, even after UV illumination, that no Cr^{4+} centers of the type observed in BSO:Cr are found.

After 413 nm illumination, the sample was exposed to 647.1 nm laser light for 30 minutes. This treatment leads to a nearly complete recovery of the intensity of the Cr^{3+} EPR lines as shown in Fig. 4 (spectrum c). This suggests that the illumination with 647 nm is able to excite the electrons from the traps back to the conduction band and make them available to regenerate the trigonal Cr^{3+} defects, making it a reversible process.

C. Optical absorption spectra

To gain further understanding of these processes we have performed parallel optical absorption measurements of the BSO:Cr+P crystals. For comparison the optical absorption measurements were also performed on BSO: Cr, BSO: P and non-doped BSO crystals. The measurements were carried out at T = 90 K before and after near-UV irradiation, and then also after a subsequent red light excitation. As one can see in Fig. 5, before the UV

irradiation (curve a) the spectra consist of a single, relatively weak but well-defined band around 550 nm. After exposing the sample to near UV light (curve b), new bands appear: a weak band around 470 nm, a broader intense band with maximum at 675 nm and a very broad feature in the near-infrared showing up as a tail up to ~1400 nm. In correlation with the light-induced EPR results (see Fig. 4) these belong to the products of light-induced charge transfer, and as discussed below Cr^{4+} and/or P^{4+} containing defects are possible candidates. Subsequent red light illumination was found, also in the absorption spectrum (curve c of Fig. 5), to lead to a nearly full recovery of the initial state, with complete bleaching of the 675 nm band and of the long wavelength tail. However, the weak band at 470 nm is surviving and thus belongs to a separate species.

It is useful at this point to compare the above results with the absorption spectrum of chromium-only doped BSO, shown as inset graph of Fig. 5. In the annealed BSO:Cr crystal the broad band at ~490 nm was attributed to the antisite Bi_M^{4+} defect,[7] which is absent in P co-doped crystals, as we also observed in EPR. The band with pronounced substructure around 750 nm is typical for Cr^{4+} tetrahedrally coordinated with oxygen ligands [15-18,25,26] and is attributed to the Cr_{Si}^{4+} defect. Clearly, this band is totally absent in the as-grown BSO:Cr+P crystals. Also, the new band appearing after near-UV excitation in the co-doped crystals is quite different in position (675 nm vs. 750 nm) and in line shape, and is found to disappear upon warming to RT. The light-induced defect in BSO:Cr+P related to this new band is therefore not the Cr^{4+} center as found in as-grown BSO:Cr. This correlates well with the EPR results showing that the Cr_{Si}^{4+} defects remain absent in BSO:Cr+P even after near-UV excitation.

4. DISCUSSION

We identified the new EPR spectra in BSO:Cr+P crystals with a defect containing the trivalent $Cr^{3+}(3d^3, {}^4F)$ ion, in agreement with the effective spin S=3/2 and consistent with the SH parameters. However, the local structure of the defect remains to be considered.

An identification as Cr^{3+} in a distorted octahedral crystal field ($3d^3$ configuration, ${}^4A_2({}^4F)$ ground state) appears tempting, and the Bi^{3+} site in this host may seem to offer such an environment. A related case has been reported by Bravo *et al.*[20] in the

scintillator material $Bi_4Ge_3O_{12}$ in which Cr^{3+} is found in distorted octahedral coordination at the Bi crystal site with <111> trigonal symmetry (coexisting with the dominant chromium center: Cr^{4+} at the Ge site). For Cr^{3+}, they reported slightly anisotropic g-values ($g_{//} = 1.958$, $g_{\perp} = 1.963$) and a larger ZFS value ($B_2^0 = 0.322$ cm^{-1}) than observed here. A major objection in the present case is the fact that the bismuth site in the sillenites, with seven oxygen neighbors, possesses lower than trigonal symmetry as illustrated in Fig. 1(a). This was also observed in an optical study[36] using Eu^{3+} ions as probes replacing Bi^{3+}. Such a low symmetry perturbation in the first shell may be expected to induce a larger ZFS and more parameters would be required for accurate fitting. This is quite unlikely taking into account that, up to W-band frequencies, the EPR analysis failed to detect such a deviation from trigonal symmetry.

Therefore, the alternative of a Cr^{3+} in a tetrahedral site has to be considered. It is now straightforward to obtain the observed defect symmetry by a trigonal perturbation along a <111> direction. The latter could either result from a nearby associated defect, e.g., a vacancy or an impurity ion, or could occur spontaneously. Indeed, a Jahn-Teller type distortion of the surroundings can occur for an ion with an orbitally degenerate ground state, which is the case of $Cr^{3+}(3d^3, {}^4F)$ ion possessing a 3-fold degenerate ${}^4T_1$ ground level in tetrahedral coordination. A distortion along a low-symmetry coordinate combined with spin orbit coupling further splits the ${}^4T_1$ ground state, leaving an effective spin quartet (S = 3/2) lowest in energy with expected SH parameters very similar to those determined here.[35]

As discussed below, the combined EPR and optical data lead us to believe that the trigonal perturbation results from a nearby defect. An oxygen vacancy in the Cr^{3+} containing tetrahedron would yield the observed <111> trigonal symmetry, but with such a drastic perturbation of the coordination one would expect a much larger ZFS. In fact, association with a P^{5+} dopant ion, as depicted in Fig. 1(b), provides a more plausible explanation for the symmetry of the Cr^{3+} center in BSO:Cr+P. Indeed, phosphorus is present at high concentration in the crystal and is known to substitute for Si-ions with tetrahedral oxygen coordination. At the measured relative concentration [P]/[Si] = 2.2 %, the probability to find a P^{5+} ion at a nearest-neighbor Si-site relative to that of the Cr^{3+} ion

(Si-Si distance in BSO: 8.75 Å) is very high. The two dopants with opposite net charge might be even preferentially associated.[37] As mentioned before, the strong donor character of the P-dopant would provide for efficient conversion to trivalent chromium. The pairing at such a distance is compatible with the relatively weak perturbation leading to a modest ZFS accompanied by a g-anisotropy, too small to be detected in combination with the large EPR line widths.

Near-UV illumination, at 413 nm, is able to change the charge state of dopants and defects by one, exciting an electron from the defect to the conduction band, or from the valence band to the defect, or else by electron or hole trapping after interband excitation. The photon energy is sufficient for any of these transitions. Then, starting from Cr^{3+}, one should produce either Cr^{2+} or Cr^{4+} centers (or both). However, no new EPR signals appear in the spectra that could be related to either one of these valences. The Cr^{2+} ion has not yet been reported as impurity in this type of oxides, as far as we know, and we have found no evidence for its presence. As shown by the absence of both the isotropic EPR line at $g \cong 1.938$ and the optical band centered at 750 nm, the Cr_{Si}^{4+} defect existing in BSO:Cr does not appear in the co-doped BSO:Cr+P crystal and also is not produced by near-UV illumination. Either no Cr^{4+} centers are formed at all or, more probably, the resulting Cr^{4+} centers possess lower symmetry than tetrahedral, which is consistent with the proposed Cr^{3+}-P^{5+} association. Such a Cr^{4+} center perturbed by a neighboring P^{5+} ion may contribute to the light induced 675 nm absorption band. The shift in transition energy relative to the Cr_{Si}^{4+} defect (see insert in Fig. 5) seems acceptable, as seen by comparison with data from 4-fold oxygen coordinated Cr^{4+} ions in lower symmetry sites centers in $LiAlO_2$ and $LiGaO_2$, with absorption maxima in the 600-700 nm range.[38] Also, it was checked that this 675 nm absorption band is not produced by near-UV excitation in BSO:Cr in the absence of phosphorus. However, it cannot be excluded that the light-induced absorption spectrum is partly or completely corresponding to the broad 1.8 eV band reported[10] for the trapped-electron P^{4+} defect in BSO:P. The final assignment of the induced absorption spectrum requires further investigation.

5. CONCLUSION

We have shown that co-doping of BSO with chromium and phosphorus can strongly influence the properties of the chromium centers in charge state and surrounding, and drastically alters the optical spectra of the material, which is attractive for the engineering of the photorefractive properties. The observed anisotropic EPR spectra give for the first time unambiguous evidence that chromium can be incorporated into the $Bi_{12}SiO_{20}$ crystal in the Cr^{3+} valence state substituting for Si^{4+} at the tetrahedral metal site. The trigonal perturbation is attributed to the presence of a P^{5+} ion in a nearest-neighbor Si lattice site. Near-UV illumination results in a charge transfer process involving the Cr^{3+} defects, which is reversible by red light excitation. The knowledge of this charge transfer process can be exploited to optimize the functionality of bismuth sillenite materials.

ACKNOWLEDGMENTS

Financial support is kindly acknowledged both from the Research Foundation – Flanders (FWO) in the framework of the group project G.0116.06N, and from the Hercules Foundation of Flanders, Belgium (contract AUHA013). H. Vrielinck acknowledges a postdoctoral fellowship and V. Marinova a visiting postdoctoral fellowship with the F.W.O. We are grateful to the Crystal Growth Laboratory of the Institute of Solid State Physics, Sofia, Bulgaria, for the growth of the single crystals supported by Bulgarian National Fund project # TK-X-1715/07. We thank Peter Gast at Leiden University for support in W-band ENDOR measurements.

REFERENCES

1. Y. H. Ja, Opt. Commun. **42**, 377 (1982).
2. M. P. Georges, V. S. Scauflaire, P. C. Lemaire, Appl. Phys. B **72**, 761 (2001).
3. E. A. Barbosa, R. Verzini, J. F. Carvalho, Opt. Commun. **263**, 189 (2006).
4. M. R. R. Gesualdi, D. Soga, M. Muramatsu, Opt. Laser Technol. **39**, 98 (2007).
5. E. A. Barbosa, A. O. Preto, D. M. Silva, J. F. Carvalho, N. I. Morimoto, Opt. Commun. **281**, 408 (2008).
6. K. Buse, Appl. Phys. B **64**, 391 (1997).
7. B. C. Grabmaier, R. Oberschmid, Phys. Status Solidi (a) **96**, 199 (1986).
8. H. Marquet, M. Tapiero, J. C. Merle, J. P. Zielinger, and J. C. Launay, Opt. Mater. **11**, 53 (1998).
9. V. Marinova, Opt. Mater. **15**, 149 (2000).
10. J. S. McCullough, A. Harmon, J. J. Martin, J. J. Martin, M. T. Harris, J. J. Larkin, J. Appl. Phys. **78**, 2010 (1995).
11. A. V. Egorysheva, V. V. Volkov, V. M. Skorikov, Inorg. Mater. **31**, 348 (1995).
12. H.-J. Reyher, U. Hellwig, O. Thiemann, Phys. Rev. B **47**, 5638 (1993).
13. B. Briat, H. J. Reyher, A. Hamri, N. G. Romanov, J. C. Launay, F. Ramaz, J. Phys.: Condens. Matter **7**, 6951 (1995).
14. I. Ahmad, V. Marinova, E. Goovaerts, Phys. Rev. B **79**, 033107 (2009).
15. W. Wardzynski , H, Szymczak, K. Pataj, T. Lukasiewicz, J. Zmija, J. Phys. Chem. Solids **43**, 767 (1982).
16. C. Coya, J. L. G. Fierro, C. Zaldo, J. Phys. Chem. Solids **58**, 1461 (1997).
17. J. S. McCullough, A. L. Harmon Bauer, C. A. Hunt, J. J. Martin, J. Appl. Phys. **90**, 6017 (2001).
18. A.V. Egorysheva , V.V. Volkov, C. Coya, C. Zaldo, Phys. Status Solidi (b) **207**, 283 (1998).

19. W. Wardzynski, H. Szymczak, J. Phys. Chem. Solids **45**, 887 (1984).

20. D. Bravo, F. J. Lopez, Opt. Mater. **13**, 141 (1999).

21. F. J. Lopez, E. Moya, C. Zaldo, Solid State Commun. **76**, 1169 (1990).

22. W. Wardzynski , T. Lukasiewicz, J. Zmija, Opt. Commun. **30**, 203 (1979).

23. A. M. Darwish, R. Silz, R. Copeland, P. Venkateswarlu, J. Choi, R. Metzl, W. S. Wang, M. D. Aggarwal, A. Williams, SPIE Proc. **2849**, 67 (1996).

24. V. Tassev, M. Gospodinov, M. Veleva, Opt. Mater. **13**, 249 (1999)

25. A. V. Egorysheva, V. I. Burkov, Yu. F. Kargin , A. Y. Vasil'ev, V. V. Volkov, V. M. Skorikov, Inorg. Mater. **37**, 817 (2001).

26. A. A. Nechitailov, M. V. Krasin'kova, E. V. Mokrushina, A. A. Petrov, N. F. Kartenko, V. V. Prokofév, Inorg. Mater. **36**, 820 (2000).

27. B. Briat, V. G. Grachev, G. I. Malovichko, O. F. Schirmer, and M. Wöhlecke, in *Photorefractive Materials and Their Applications*, edited by P. Günter and J.-P. Huignard (Springer-Verlag, Berlin, 2007), Vol. 2, pp. 9–49.

28. S. C. Abrahams, J. L. Bernstein, C. Svensson, J. Chem. Phys. **71**, 788 (1979); S. C. Abrahams, P. B. Jamieson, J. L. Bernstein, *ibid.* **47**, 4034 (1967).

29. P. Sveshtarov, M. Gospodinov, J. Cryst. Growth **113**, 186 (1991).

30. J. Glerup, H. Weihe, Acta Chem. Scand. **45**, 444 (1991).

31. H. J. Von Bardeleben, J. Phys. D: Appl. Phys. **16**, 29 (1983).

32. M. G. Jani, L. E. Halliburton, J. Appl. Phys. **64**, 2022 (1988).

33. A. Abragam, B. Bleaney, *Electron Paramagnetic Resonance of Transition Ions* (Clarendon Press, Oxford, 1970).

34. See Ref. 33, pp. 430-434; also: J. R. Pilbrow, *Transition Ion Electron Paramagnetic Resonance* (Clarendon Press, Oxford, 1990), pp. 120-125.

35. See Ref. 33, p. 469; J. Schneider, B. Dischler, A. Räuber, Solid State Commun. **5**, 6003 (1967); J. C. M. Henning, J. Liebertz, R. P. Van Stapele, J. Phys. Chem. Solids **28**, 1109 (1967); J. J. Krebs, G. H. Stauss, Phys. Rev. B **15**, 17 (1977).

36. C. Cascales, P. Porcher, J. Fernández, A. Oleaga, R. Balda, E. Diéguez, J. Alloys Compounds **323**&**324**, 260 (2001).

37. Unfortunately, our attempts to measure a possible ^{31}P hyperfine coupling using different advanced EPR techniques have not been successful, due to unfavorable spin relaxation properties. Detection of ^{31}P (I = ½, 100% abundance) hyperfine coupling was attempted using X-band electron spin echo envelope modulation (ESEEM), CW Q-band ENDOR and also pulsed W-band ENDOR.

38. S. Kück, S. Hartung, Chem. Phys. **240**, 387 (1999).

FIGURE CAPTIONS

FIG. 1. (a) View along a <111> direction of the SiO_4 tetrahedron (fourth oxygen hidden) connected to one of the neighboring BiO_7 polyhedra. The low symmetry bismuth site can be viewed as a distorted square pyramid containing the Bi^{3+} ion in the base plane with two (more distant) oxygen ions opposite to the top of the pyramid. (b) Model of the chromium defect in the cubic BSO crystal with the Cr^{3+} and P^{5+} ions in nearest neighbor tetrahedral Si^{4+} sites (BiO_7 polyhedra omitted).

FIG. 2. (a) X-band (T = 10 K), (b) Q-band (T = 6 K), and (c) W-band (T = 12 K) EPR spectra of as-grown BSO:Cr+P with the magnetic field in a {110} plane, close to a <111> crystal direction. A number of transitions of the Cr^{3+} related spectrum are marked by arrows. In (c) the inset shows the spectrum of BSO: Cr for comparison.

FIG. 3. W-band angular variation of the EPR resonance positions of the Cr^{3+} defect in BSO:Cr +P at 12 K when the magnetic field is applied in a {110} plane. The solid and half-open diamonds correspond to the experimental data for the allowed and forbidden transitions, respectively. The open circles show the computed field positions with their size representing the calculated transition probabilities.

FIG. 4. W-band EPR spectrum of the Cr^{3+} defect in BSO:Cr+P measured at 12 K (a) before illumination (b) after 20 min illumination with 413 nm laser light and (c) after a consecutive 30 minutes illumination with 647 nm laser light.

FIG. 5. Optical absorption spectra of the BSO:Cr+P crystal measured at 90 K: (a) after annealing, (b) after near-UV irradiation at 413 nm showing the conversion of the chromium defect and (c) after consecutive red illumination at 647 nm. Inset: spectra of (d) annealed BSO:Cr, and (e) BSO: P crystals.

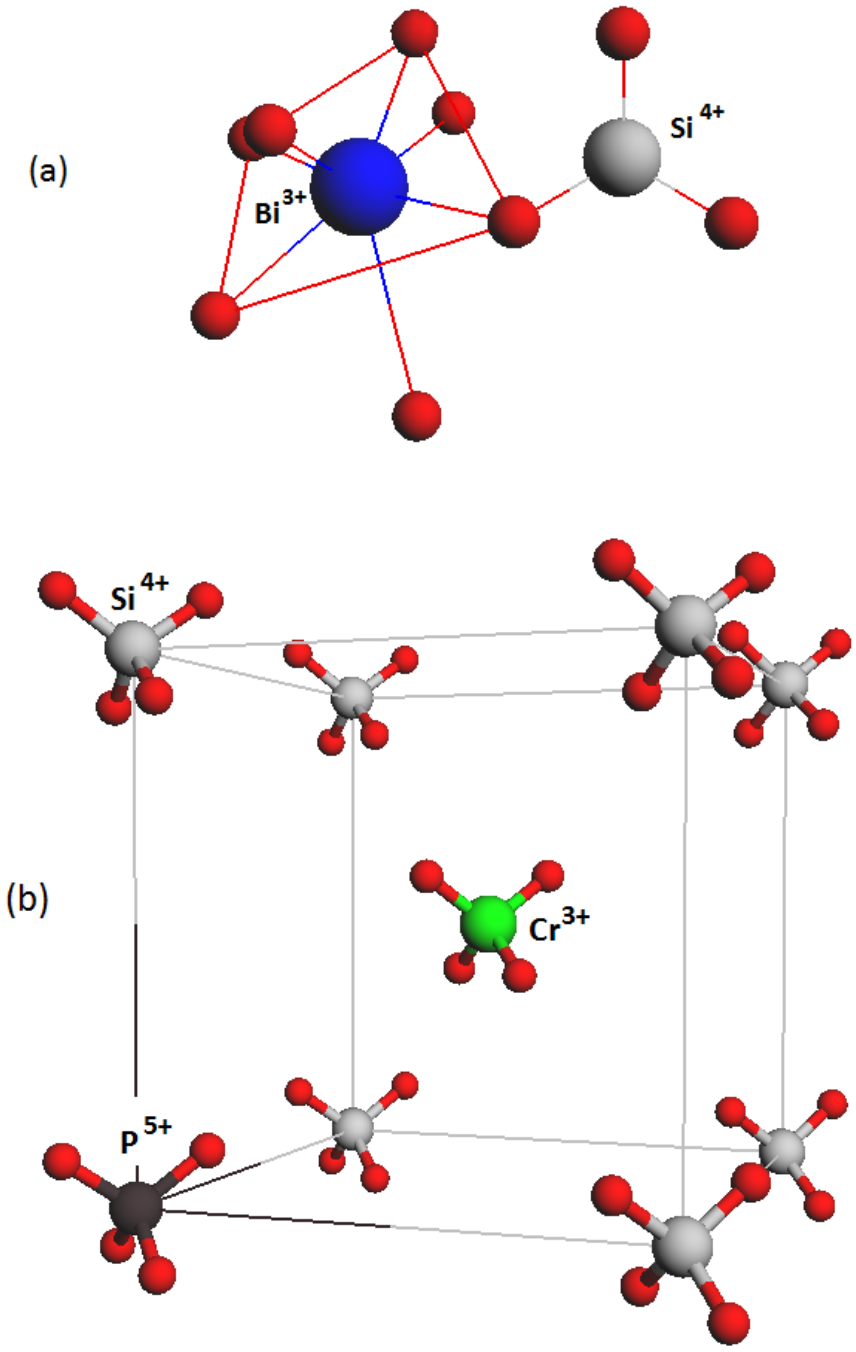

FIG. 1. (a) View along a <111> direction of the SiO_4 tetrahedron (fourth oxygen hidden) connected to one of the neighboring BiO_7 polyhedra. The low symmetry bismuth site can be viewed as a distorted square pyramid containing the Bi^{3+} ion in the base plane with two (more distant) oxygen ions opposite to the top of the pyramid. (b) Model of the chromium defect in the cubic BSO crystal with the Cr^{3+} and P^{5+} ions in nearest neighbor tetrahedral Si^{4+} sites (BiO_7 polyhedra omitted).

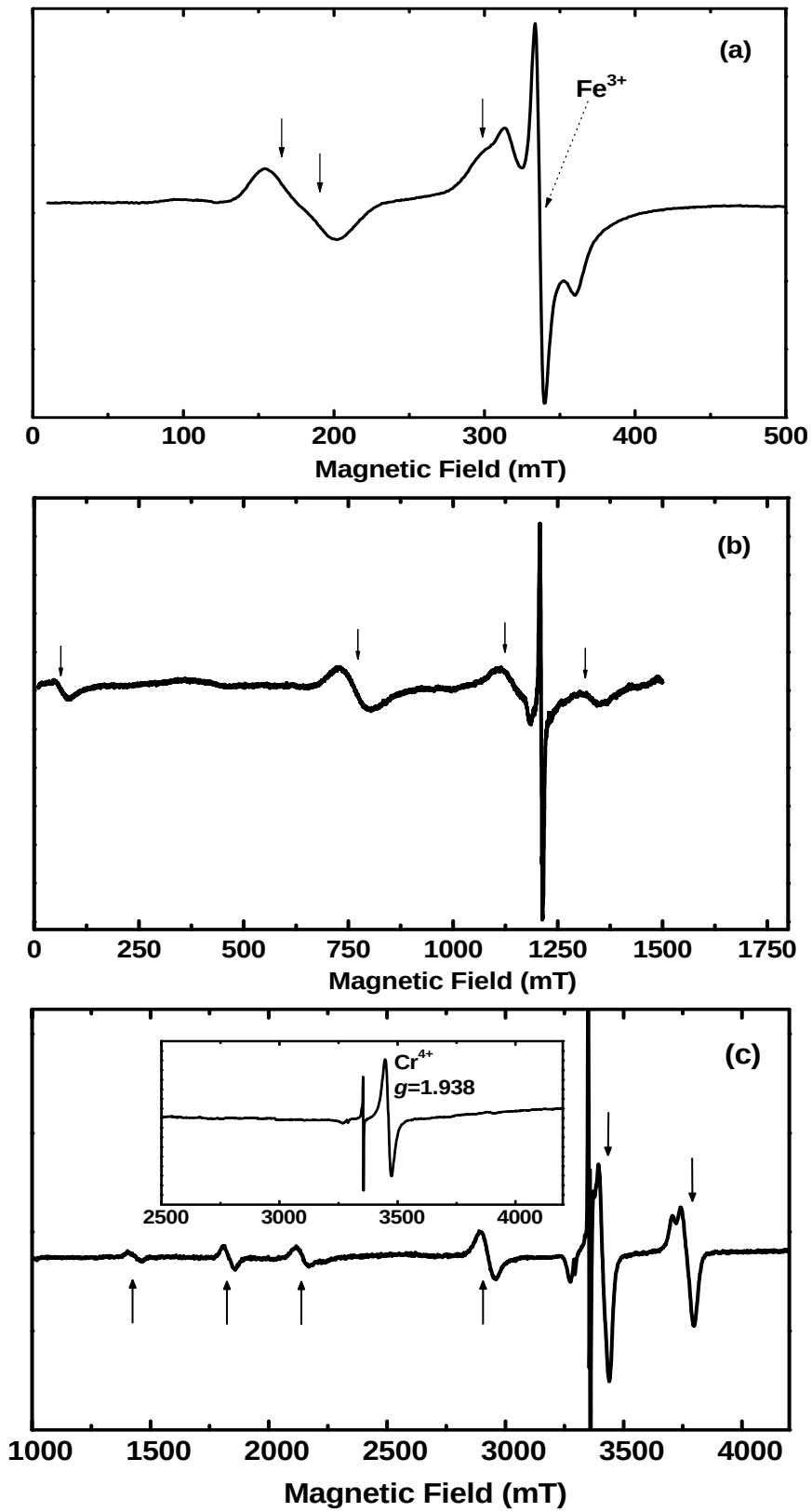

FIG. 2. (a) X-band (T = 10 K), (b) Q-band (T = 6 K), and (c) W-band (T = 12 K) EPR spectra of as-grown BSO:Cr+P with the magnetic field in a {110} plane, close to a <111> crystal direction. A number of transitions of the Cr^{3+} related spectrum are marked by arrows. In (c) the inset shows the spectrum of BSO: Cr for comparison.

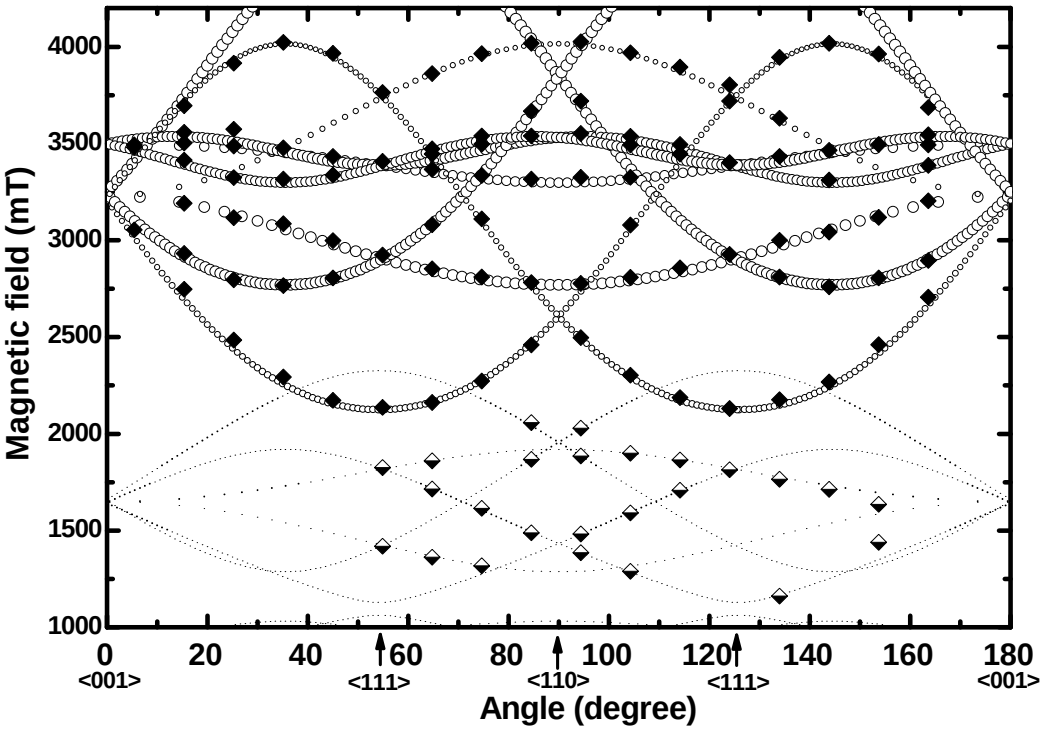

FIG. 3. W-band angular variation of the EPR resonance positions of the Cr^{3+} defect in BSO:Cr +P at 12 K when the magnetic field is applied in a {110} plane. The solid and half-open diamonds correspond to the experimental data for the allowed and forbidden transitions, respectively. The open circles show the computed field positions with their size representing the calculated transition probabilities.

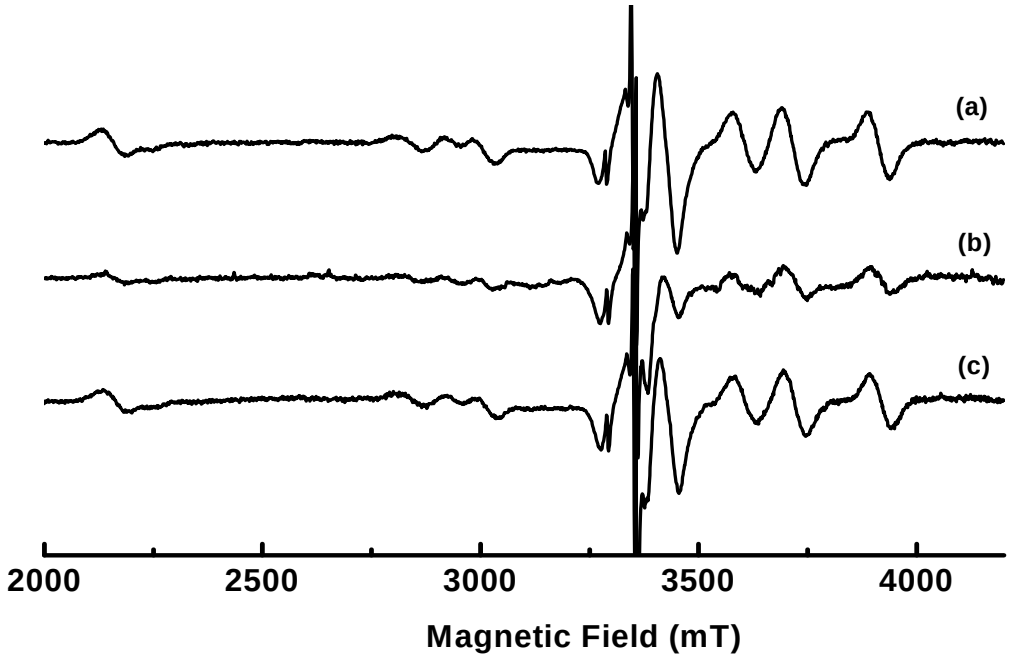

FIG. 4. W-band EPR spectrum of the Cr^{3+} defect in BSO:Cr+P measured at 12 K (a) before illumination (b) after 20 min illumination with 413 nm laser light and (c) after a consecutive 30 minutes illumination with 647 nm laser light.

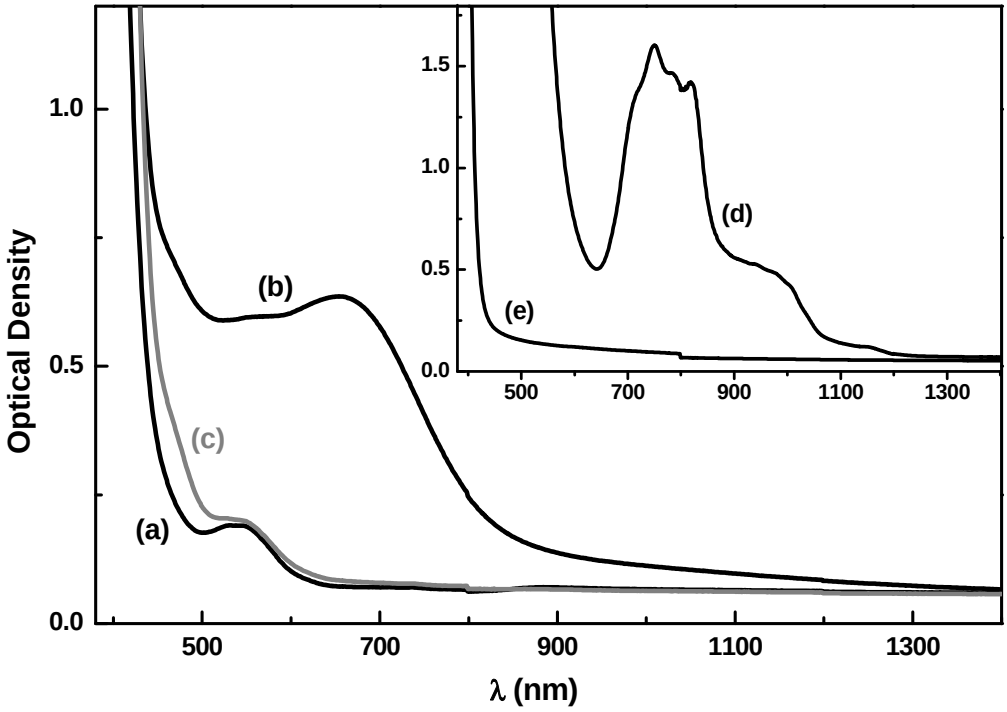

FIG. 5. Optical absorption spectra of the BSO:Cr+P crystal measured at 90 K: (a) after annealing, (b) after near-UV irradiation at 413 nm showing the conversion of the chromium defect and (c) after consecutive red illumination at 647 nm. Inset: spectra of (d) annealed BSO:Cr, and (e) BSO: P crystals.